

Supplemental Material for “Columnar order and Ashkin-Teller criticality in mixtures of hard-squares and dimers”

Kabir Ramola,¹ Kedar Damle,² and Deepak Dhar²

¹*Laboratoire de Physique Théorique et Modèles Statistiques, UMR 8626, Université Paris-Sud 11 and CNRS, Bâtiment 100, Orsay F-91405, France*

²*Tata Institute of Fundamental Research, 1 Homi Bhabha Road, Mumbai, India 400005*

In this document we present details of our Monte Carlo algorithm and additional results from our simulations which support the key findings highlighted in the main text.

TRANSFER-MATRIX BASED ALGORITHM

Update Scheme

To simulate the system of dimers and squares on the square lattice, we use the following transfer-matrix based Monte Carlo algorithm which is a variant of the technique developed in Refs. [1–5]. Our variant is designed to ensure that we can work directly in the full-packing limit if needed. In our scheme, we update all objects fully contained in a $2 \times N$ track (two adjacent rows/columns of plaquettes) at once, with the correct weights in the partition function. The steps involved in each update are as follows:

- We empty out all objects that are fully contained within a randomly chosen $2 \times N$ track (horizontal or vertical).
- The remaining objects either lie outside the chosen track (this includes objects which share an edge with the long boundary of the track) or protrude partially into the track. The latter class of objects, which protrude partially into the track, provide excluded-volume constraints that need to be respected when the track is refilled.
- To refill the track with objects lying entirely within the track, we compute the partition function of the track subject to the constraints imposed by objects that protrude into the track. This is done using a standard transfer matrix technique.
- Using this partition function, we generate a configuration with the correct Boltzmann weight consistent with the constraints, and re-populate the track. We summarize these steps in Fig. 1 below.

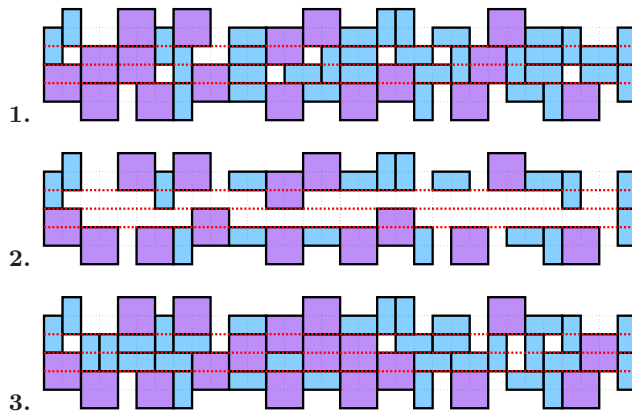


FIG. 1: Steps in the transfer-matrix based algorithm. **1.** The initial configuration of the randomly chosen $2 \times N$ track (red dashed lines), showing objects lying completely within it, objects lying immediately outside it (but sharing an edge with the track), and objects protruding into the track. **2.** All objects lying fully within the track are evaporated. We leave unchanged all objects that lie completely outside the track (not shown) or objects lying immediately outside the track (sharing an edge with the track without protruding into the track), as well as objects that protrude into the track. **3.** The track is re-populated with a new configuration of objects lying entirely within the track, subject to the excluded volume constraints imposed by objects protruding into the track.

To evaluate the weights of the allowed configurations for the purpose of refilling a track, we need to calculate the restricted partition function of this track subject to constraints imposed by objects protruding into the track. We do this by using a standard transfer matrix technique. Below we provide details of this update for a horizontal track.

Details of the Transfer Matrices

We break up the track into a sequence of two-plaquette “rungs”, defined as two vertically adjacent plaquettes. After the track is emptied of all objects lying completely within it, these rungs still have areas covered by objects protruding into the track from above and below (as shown in **2.** of Fig. 1). These protrusions preclude the occupation of some objects on the rung, and thereby provide constraints on which objects can be re-populated. The four possible types of protrusions (represented by shaded areas) on a given rung are shown in Fig. 2. Based on this underlying “morphology”, we assign an index σ to each rung, with $\sigma = 1, 2, 3, 4$ chosen with the convention of Fig. 2.

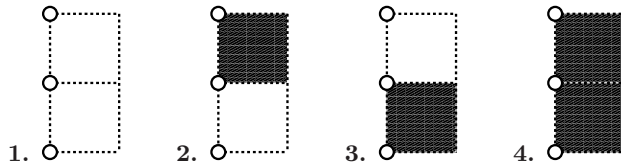


FIG. 2: The four possible underlying morphologies $\sigma = 1, 2, 3, 4$ of a two-plaquette rung, arising from objects protruding into the track from above and below (represented by the shaded areas). $\sigma = 4$ corresponds to a complete blockade.

Next, in order to fill the rung with objects, we focus on the “state” C of a rung, the ways in which objects can be placed on this rung. When the underlying morphology is ignored, there are **six** possible ways of filling a two-plaquette rung, as shown in Fig. 3.

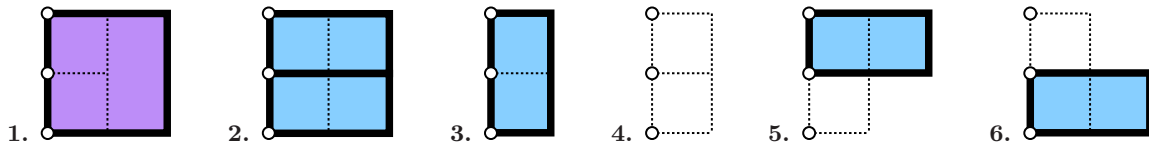


FIG. 3: The six possible states of a two-plaquette rung.

To unambiguously assign objects to each rung, we use the convention that objects are on the rung, if their left edge coincides with the left edge of the rung (represented by open circles in Fig. 3). Our convention is also designed to ensure that the allowed states are influenced *only* by the morphology of the given rung and the one immediately to the right. When the underlying morphology is considered, not all states are allowed. For example, state $C = 3$ is disallowed if the morphology of the rung is $\sigma = 2, 3, 4$, the state $C = 6$ is disallowed if the morphology of the rung OR of the rung immediately to the right is $\sigma = 3, 4$, and so on.

We next construct the partition function of the track subject to these constraints and also the excluded volume constraints provided by the objects on the track. Our transfer matrix formalism transfers the state of a two-plaquette rung to the next two-plaquette rung to its *left*, subject to these constraints. So, let $Z_n(C', \sigma')$ be the partition function of an n -rung track, where the leftmost rung is filled with the state C' , and has an underlying morphology σ' . Then, the partition function of the $(n + 1)$ -rung track, $Z_{n+1}(C, \sigma)$ is given by the recursion relation:

$$Z_{n+1}(C, \sigma) = \sum_{C'} T_{\sigma, \sigma'}(C, C') Z_n(C', \sigma'), \quad (1)$$

where $T_{\sigma, \sigma'}(C, C')$ is a 6×6 transfer matrix, consistent with the excluded volume constraints of C and C' and also with the constraints provided by the underlying morphology σ, σ' . We therefore have 16 possible transfer matrices, based on these indices σ, σ' . However, we note that if there is a complete disruption in the track ($\sigma = 4$), the partition function of the track breaks up into a product over partition functions of open chains. We deal with these cases separately since, as we show later, the computational cost is greatly reduced in this case.

Hence, based on the possible combinations $\sigma, \sigma' = 1, 2, 3$ (shown in Fig. 4), there are **nine** possible transfer matrices. We list them below:

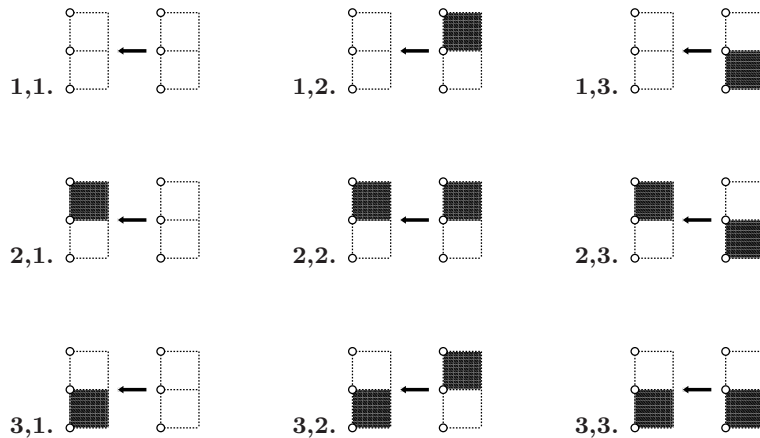


FIG. 4: The nine possible transfers between two rungs, based on the combinations $\sigma, \sigma' = 1, 2, 3$.

$$\begin{aligned}
\mathcal{T}_{1,1} &= \begin{pmatrix} 0 & 0 & 0 & z_s & 0 & 0 \\ 0 & 0 & 0 & z_d^2 & 0 & 0 \\ z_d & z_d & z_d & z_d z_v^2 & z_d z_v & z_d z_v \\ 1 & 1 & 1 & z_v^2 & z_v & z_v \\ 0 & 0 & 0 & z_d z_v & 0 & z_d \\ 0 & 0 & 0 & z_d z_v & z_d & 0 \end{pmatrix}, & \mathcal{T}_{1,2} &= \begin{pmatrix} 0 & 0 & 0 & 0 & 0 & 0 \\ 0 & 0 & 0 & 0 & 0 & 0 \\ 0 & 0 & 0 & z_d z_v & 0 & z_d \\ 0 & 0 & 0 & z_v & 0 & 1 \\ 0 & 0 & 0 & 0 & 0 & 0 \\ 0 & 0 & 0 & z_d & 0 & 0 \end{pmatrix}, & \mathcal{T}_{1,3} &= \begin{pmatrix} 0 & 0 & 0 & 0 & 0 & 0 \\ 0 & 0 & 0 & 0 & 0 & 0 \\ 0 & 0 & 0 & z_d z_v & z_d & 0 \\ 0 & 0 & 0 & z_v & 1 & 0 \\ 0 & 0 & 0 & z_d & 0 & 0 \\ 0 & 0 & 0 & 0 & 0 & 0 \end{pmatrix}, \\
\mathcal{T}_{2,1} &= \begin{pmatrix} 0 & 0 & 0 & 0 & 0 & 0 \\ 0 & 0 & 0 & 0 & 0 & 0 \\ 0 & 0 & 0 & 0 & 0 & 0 \\ 1 & 1 & 1 & z_v^2 & z_v & z_v \\ 0 & 0 & 0 & 0 & 0 & 0 \\ 0 & 0 & 0 & z_d z_v & z_d & 0 \end{pmatrix}, & \mathcal{T}_{2,2} &= \begin{pmatrix} 0 & 0 & 0 & 0 & 0 & 0 \\ 0 & 0 & 0 & 0 & 0 & 0 \\ 0 & 0 & 0 & 0 & 0 & 0 \\ 0 & 0 & 0 & z_v & 0 & 1 \\ 0 & 0 & 0 & 0 & 0 & 0 \\ 0 & 0 & 0 & z_d & 0 & 0 \end{pmatrix}, & \mathcal{T}_{2,3} &= \begin{pmatrix} 0 & 0 & 0 & 0 & 0 & 0 \\ 0 & 0 & 0 & 0 & 0 & 0 \\ 0 & 0 & 0 & 0 & 0 & 0 \\ 0 & 0 & 0 & z_v & 1 & 0 \\ 0 & 0 & 0 & 0 & 0 & 0 \\ 0 & 0 & 0 & 0 & 0 & 0 \end{pmatrix}, \\
\mathcal{T}_{3,1} &= \begin{pmatrix} 0 & 0 & 0 & 0 & 0 & 0 \\ 0 & 0 & 0 & 0 & 0 & 0 \\ 0 & 0 & 0 & 0 & 0 & 0 \\ 1 & 1 & 1 & z_v^2 & z_v & z_v \\ 0 & 0 & 0 & z_d z_v & 0 & z_d \\ 0 & 0 & 0 & 0 & 0 & 0 \end{pmatrix}, & \mathcal{T}_{3,2} &= \begin{pmatrix} 0 & 0 & 0 & 0 & 0 & 0 \\ 0 & 0 & 0 & 0 & 0 & 0 \\ 0 & 0 & 0 & 0 & 0 & 0 \\ 0 & 0 & 0 & z_v & 0 & 1 \\ 0 & 0 & 0 & 0 & 0 & 0 \\ 0 & 0 & 0 & 0 & 0 & 0 \end{pmatrix}, & \mathcal{T}_{3,3} &= \begin{pmatrix} 0 & 0 & 0 & 0 & 0 & 0 \\ 0 & 0 & 0 & 0 & 0 & 0 \\ 0 & 0 & 0 & 0 & 0 & 0 \\ 0 & 0 & 0 & z_v & 1 & 0 \\ 0 & 0 & 0 & z_d & 0 & 0 \\ 0 & 0 & 0 & 0 & 0 & 0 \end{pmatrix}. \quad (2)
\end{aligned}$$

It is useful to note that our convention of assigning objects to the rungs, leads to factors of z_v appearing asymmetrically in various entries of the transfer matrices. For example $\mathcal{T}_{1,1}(4,5) = z_v$, since this leaves a vacancy at the bottom of the rung transferred from.

Partition Function

If there are no complete blockades on the track, the partition function is that of a closed chain given by

$$Z_{\text{track}}^{\text{closed}} = \text{Tr}(\mathcal{T}_L \dots \mathcal{T}_3 \mathcal{T}_2 \mathcal{T}_1). \quad (3)$$

where L is the size of the lattice and the matrices \mathcal{T}_i are chosen according to the underlying morphology as described above. Here $\mathcal{T}_1 = \mathcal{T}_{\sigma_2, \sigma_1}$, $\mathcal{T}_2 = \mathcal{T}_{\sigma_3, \sigma_2} \dots$, $\mathcal{T}_L = \mathcal{T}_{\sigma_1, \sigma_L}$.

If one or more of the rungs on the track is completely blocked ($\sigma = 4$), then the partition function of the track is given by a product of partition functions of open chains. For an open chain where $N < L$ consecutive rungs are allowed for occupation, the partition function is given by

$$Z_{\text{track}}^{\text{open}} = \langle \mathcal{L}_{\sigma_N} | \mathcal{T}_{N-1} \dots \mathcal{T}_3 \mathcal{T}_2 \mathcal{T}_1 | \mathcal{R}_{\sigma_1} \rangle, \quad (4)$$

where σ_1 and σ_N represent the morphology of the first and N -th rung respectively. The three right vectors are given by (formally $\mathcal{R}_\sigma(C) = \mathcal{T}_{\sigma,4}(C, 4)$)

$$|\mathcal{R}_1\rangle = \begin{pmatrix} 0 \\ 0 \\ z_d \\ 1 \\ 0 \\ 0 \end{pmatrix}, \quad |\mathcal{R}_2\rangle = \begin{pmatrix} 0 \\ 0 \\ 1 \\ 0 \\ 0 \\ 0 \end{pmatrix}, \quad |\mathcal{R}_3\rangle = \begin{pmatrix} 0 \\ 0 \\ 0 \\ 1 \\ 0 \\ 0 \end{pmatrix}, \quad (5)$$

and the three left vectors are given by (formally $\mathcal{L}_\sigma(C) = \mathcal{T}_{4,\sigma}(4, C)$)

$$\langle \mathcal{L}_1| = (1 \ 1 \ 1 \ z_v^2 \ z_v \ z_v), \quad \langle \mathcal{L}_2| = (0 \ 0 \ 0 \ z_v \ 0 \ 1), \quad \langle \mathcal{L}_3| = (0 \ 0 \ 0 \ z_v \ 1 \ 0). \quad (6)$$

Choosing a New Configuration

In order to choose a new configuration of objects on this track, we use the following recursive technique.

Open Chain

For an open chain, the state C_N of the leftmost rung is chosen with the probability

$$p(C_N = i) = \frac{\langle \mathcal{L}_{\sigma_N}|i\rangle \langle i|\mathcal{T}_{N-1}\dots\mathcal{T}_3\mathcal{T}_2\mathcal{T}_1|\mathcal{R}_{\sigma_1}\rangle}{\sum_i \langle \mathcal{L}_{\sigma_N}|i\rangle \langle i|\mathcal{T}_{N-1}\dots\mathcal{T}_3\mathcal{T}_2\mathcal{T}_1|\mathcal{R}_{\sigma_1}\rangle}, \quad (7)$$

where $|i\rangle$ are the standard 6×1 basis vectors. Given this state $|i\rangle$ of the leftmost rung, the state C_{N-1} of the next rung to the right, is then chosen with the probability

$$p(C_{N-1} = j) = \frac{\langle \mathcal{L}'|j\rangle \langle j|\mathcal{T}_{N-2}\dots\mathcal{T}_3\mathcal{T}_2\mathcal{T}_1|\mathcal{R}_{\sigma_1}\rangle}{\sum_j \langle \mathcal{L}'|j\rangle \langle j|\mathcal{T}_{N-2}\dots\mathcal{T}_3\mathcal{T}_2\mathcal{T}_1|\mathcal{R}_{\sigma_1}\rangle}, \quad (8)$$

where $\langle \mathcal{L}'| = \langle i|\mathcal{T}_{N-1}$, acts as the new left vector. We can then recursively populate the entire track using this procedure. Clearly, starting from a given right vector $|\mathcal{R}_{\sigma_1}\rangle$ depending on the morphology of the rightmost rung, one only needs to store the partial products $\mathcal{T}_k\dots\mathcal{T}_3\mathcal{T}_2\mathcal{T}_1|\mathcal{R}_{\sigma_1}\rangle$, of 6×1 vectors at each rung in this algorithm.

Closed Chain

For a closed chain, the state C_L of the first rung is chosen with the probability

$$p(C_L = i) = \frac{\langle i|\mathcal{T}_L\dots\mathcal{T}_3\mathcal{T}_2\mathcal{T}_1|i\rangle}{\sum_i \langle i|\mathcal{T}_L\dots\mathcal{T}_3\mathcal{T}_2\mathcal{T}_1|i\rangle}. \quad (9)$$

Given this state $|i\rangle$ of the first rung, the state C_{L-1} of the next rung to the right is then chosen with the probability

$$p(C_{L-1} = j) = \frac{\langle i|\mathcal{T}_L|j\rangle \langle j|\mathcal{T}_{L-1}\dots\mathcal{T}_3\mathcal{T}_2\mathcal{T}_1|i\rangle}{\sum_j \langle i|\mathcal{T}_L|j\rangle \langle j|\mathcal{T}_{L-1}\dots\mathcal{T}_3\mathcal{T}_2\mathcal{T}_1|i\rangle}, \quad (10)$$

and similarly for the rest of the chain (as for the open chain), until the entire track is filled. Thus, in the case of a closed chain, one needs to store the partial products of 6×6 matrices at each rung.

We note that the algorithm described above *does not reject* any configurations. This is particularly useful when studying high density phases, where local algorithms often encounter ‘‘jamming’’. This algorithm is naturally extendable to updates of wider tracks, where the size and the number of the transfer matrices grows with the number of rows/columns considered. We also note that this algorithm is quite computationally efficient. For large lattice sizes and high densities, the probability of encountering a periodic track falls rapidly. To update a single open track, only storage of order $6L$ numbers is required in an $L \times L$ system. In the rare cases when we encounter a periodic track, we

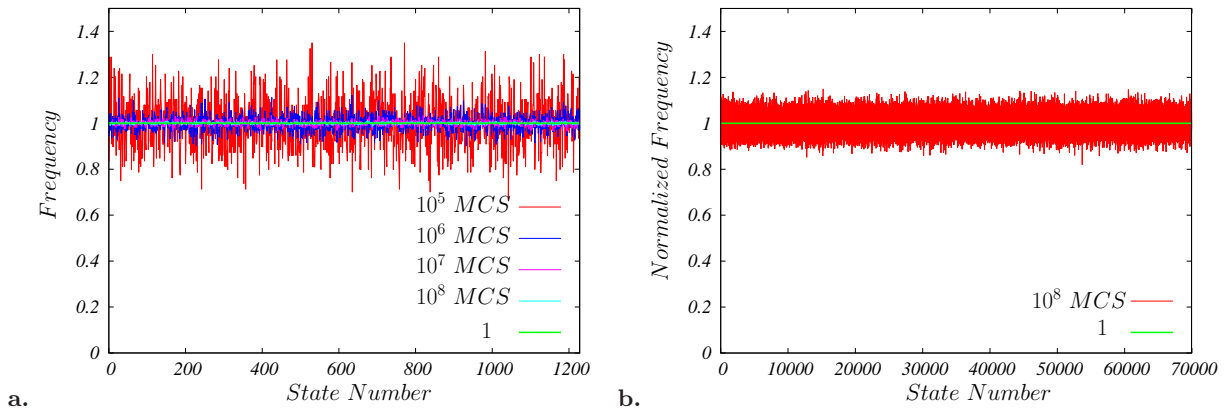


FIG. 5: Frequency of occurrence of states in a Monte Carlo simulation of a 4×4 periodic lattice **a.** at full-packing **b.** for a general $v \neq 0$ (normalized by its weight in the partition function). All states are sampled with a frequency approaching 1 as the number of Monte Carlo steps (MCS) are increased.

need storage of order $36L$ to update it. Naturally, the rarity of periodic tracks also implies that the algorithm does not change winding sectors (defined exactly as in the usual dimer model) easily for a large system. This is in principle a draw-back compared to loop algorithms or pocket-algorithms, both of which can be readily generalized for use in the present problem, and may change sectors more easily (we have not explored this in any detail).

In our simulations, we always start in the zero-winding sector, and our results for the larger values of L shown in the main text are therefore averages over the zero-winding sector. However, as is well-known in the context of interacting dimer models, the restriction to zero-winding in the microscopic model simply corresponds to periodic boundary conditions for the coarse-grained heights. Therefore, it does not change our conclusions. Finally, we note that a full Monte-Carlo sweep, requiring us to randomly choose $\mathcal{O}(L)$ different tracks and update their interior configurations, requires of order $\mathcal{O}(L^2)$ operations, making the time required comparable to that of other available schemes, while being rejection-free.

Detailed Balance and Ergodicity

Since the new configurations are chosen with the correct weights from the “restricted” partition function, this algorithm trivially satisfies the detailed balance criterion. The question of ergodicity is more subtle. To check that the algorithm samples all available states of the system, we have performed the following numerical check.

We enumerate all possible states on a 4×4 lattice with periodic boundary conditions. For the full-packing case (no vacancies), there are 1228 possible configurations of squares and dimers. Using this explicit knowledge of all the states, we monitor the frequency with which each state is sampled in our simulations. We choose activities such that all fully-packed states have unit Boltzmann weight and states with vacancies have zero weight. In this case, we have checked that for a large enough number of Monte Carlo steps, all allowed states are sampled with equal frequency. In addition we have checked that the variance of this frequency decreases as $\frac{1}{N_{MC}}$, where N_{MC} represents the number of Monte Carlo steps. In Fig. 5 **a.** we plot this frequency table for different numbers of Monte Carlo samplings.

We have also enumerated all possible states for this small sample when $v \neq 0$. In this case there are 69941 configurations of dimers, squares and vacancies available to the system. We check explicitly that each one of these states is sampled with the correct probability given by

$$p(\mathcal{C}_{dsv}^*) = \frac{w^{N_d^*} v^{N_v^*}}{\sum_{\mathcal{C}_{dsv}} w^{N_d} v^{N_v}}, \quad (11)$$

where N_d^* and N_v^* are the number of dimers and vacancies in the configuration \mathcal{C}_{dsv}^* , and N_d and N_v are the number of dimers and vacancies in the configuration \mathcal{C}_{dsv} . The sum is over all possible configurations of the system. In Fig. 5 **b.**, we plot the frequency of the occurrence of each of the 69941 configurations in our simulations, normalized by the above probability. We find that the normalized frequency of each of these states converges to 1, confirming the ergodicity of our algorithm (for small lattice sizes).

ADDITIONAL NUMERICAL EVIDENCE

Finally, we use our Monte Carlo update scheme to perform large scale simulations on the lattice gas of dimers and squares on the square lattice. Recent simulations of the hard-square lattice gas have shown the necessity of simulations on large system sizes to fully understand the nature of scaling in such hard-core systems with columnar ordering [2, 6]. The columnar ordered state is relatively unstable to the presence of vacancies, as compared to sublattice ordering, and is characterised by large correlation lengths. We therefore perform simulations on lattices of sizes up to 1024×1024 in order to fully elucidate the phase diagram of this system.

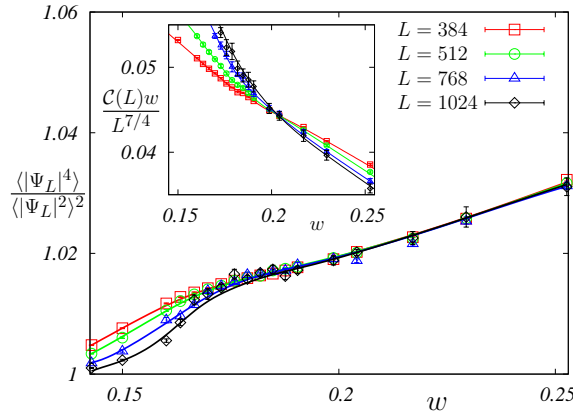


FIG. 6: Phase transition along I , the fully-packed boundary SD , ($v = 0$) corresponding to the pure squares and dimers mixture. The above figure shows the Binder-ratio $\langle |\Psi_L|^4 \rangle / \langle |\Psi_L|^2 \rangle^2$ ($\Psi_L \equiv \sum_{\vec{r}} \psi(\vec{r})$) sticking for $w > w_c^{(0)} \approx 0.198(2)$ signalling a $v = 0$ power-law columnar ordered phase for $w > w_c^{(0)}$. Inset shows $\mathcal{C}(L) = \langle |\sum_{\vec{r}} \psi(\vec{r})|^2 \rangle / L^2$ scaled by $L^{7/4}/w$ for various L . The curves cross at $w_c^{(0)}$, consistent with $\eta(w_c^{(0)}) = 1/4$.

We use the convention $v = z_v / \sqrt{z_s}$, $w = z_d / z_s^{1/4}$ and $z_s + z_d^2 + z_v^4 = 1$. In our simulations, we focus on three cuts through the phase diagram (Fig. 2 of main text) enumerated below.

I: The fully-packed boundary SD , ($v = 0$) corresponding to the pure squares and dimers mixture. We find that the system exhibits a KT transition from the square-rich columnar ordered phase to a power-law ordered dimer-rich phase above the critical point $w_c^{(0)} = 0.198(2)$. The details of the power law correlations are provided in Fig. 2 of the main text. In Fig. 6 we display the sticking of the Binder ratio $\langle |\Psi_L|^4 \rangle / \langle |\Psi_L|^2 \rangle^2$ ($\Psi_L \equiv \sum_{\vec{r}} \psi(\vec{r})$) for $w > w_c^{(0)}$ along I , signalling a power-law ordered phase in this region.

II: A trajectory passing through a generic point on the phase boundary separating the square-rich columnar ordered phase from the disordered squares-dimers-vacancy fluid phase. In our simulations, we move along the trajectory

$$z_d = \alpha z_v, \quad (12)$$

where $\alpha \approx 2.54947$. This corresponds to the trajectory $w = \alpha v(1 + w^2 + v^4)^{1/4}$. We find that in this case the transition is of second order, with a critical point at $P \equiv (w_c, v_c) = (0.1600(1), 0.0623(1))$. In Fig. 7 (a), we display the critical crossing of the columnar order parameter $\mathcal{C}(L) = \langle |\sum_{\vec{r}} \psi(\vec{r})|^2 \rangle / L^2$ scaled by $L^{2-\eta_2}$ at this critical point P , consistent with Ashkin-Teller behaviour with $\eta = \frac{1}{4}$. We find a good collapse of these curves with the scaling exponent $\nu = 1.70(5)$ (displayed in Fig. 4 of main text). In Fig. 7 (b) we display the critical crossing of the real part of the order parameter $\Re(L) = \langle [\sum_{\vec{r}} \text{Re}(\psi^2(\vec{r}))]^2 \rangle / L^2$ scaled by $L^{2-\eta_2}$, with $\eta_2 = 0.70(5)$, at this point P . Once again, these curves show a good collapse with the scaling exponent $\nu = 1.70(5)$ (displayed in the inset of Fig. 4 of the main text). These estimates of η_2 and ν satisfy $2\nu = (1 - \eta_2)^{-1}$ within errors, as argued in the main text. We also estimate $\nu = 1.70(5)$ from the scaling collapse of the Binder ratio (as displayed in Fig. 7 (c)). The error estimates are obtained by varying ν until the quality of the collapse deteriorates appreciably.

III: The boundary VS , ($w = 0$) corresponding to the hard-square lattice gas. Once again, we find that the system displays a second order phase transition to a columnar ordered state as the density of squares is increased. We display numerical results in the vicinity of this transition in Fig. 8. The first of these figures shows the columnar order parameter $\mathcal{C}(L) = \langle |\sum_{\vec{r}} \psi(\vec{r})|^2 \rangle / L^2$ scaled by $L^{7/4}$ vs. v for different values of the system size L . The curves display a sharp-crossing, which is consistent with $\eta = \frac{1}{4}$ at this transition. Using this as a prior, we obtain the precise location

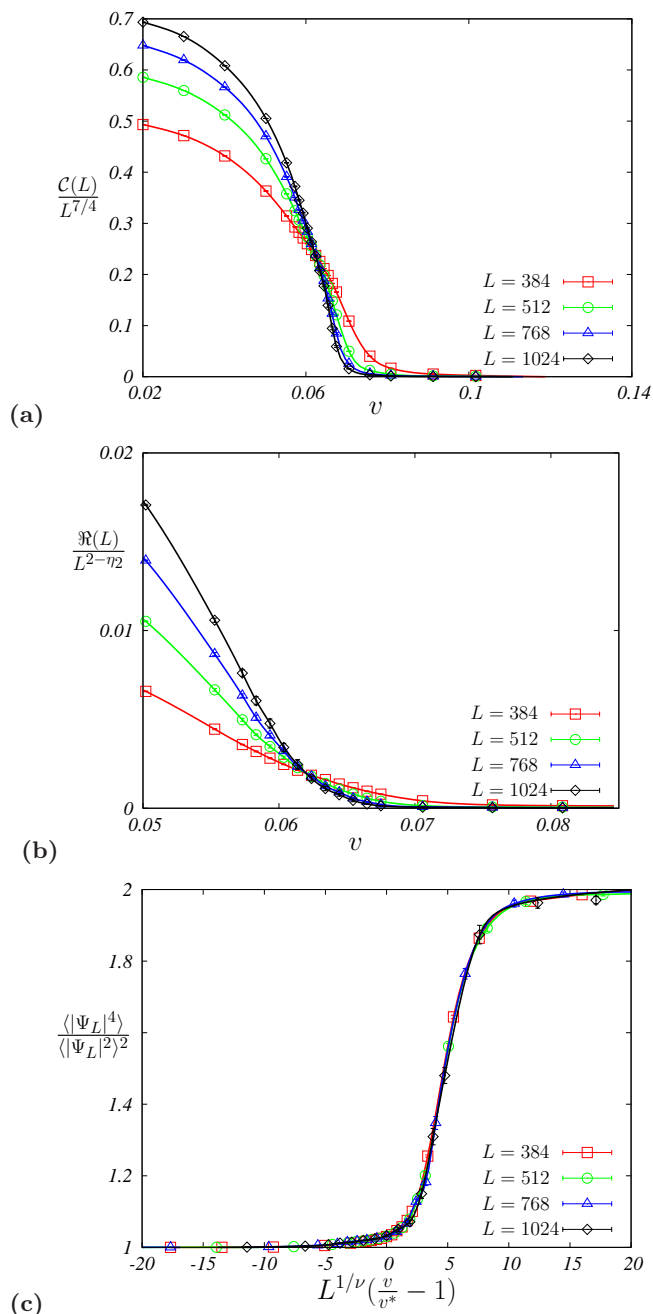


FIG. 7: Phase transition along II , defined in Eq. 12. **(a)** $\mathcal{C}(L) = \langle |\sum_{\vec{r}} \psi(\vec{r})|^2 \rangle / L^2$ scaled by $L^{7/4}$ plotted as a function of v , for different values of the system size L . The curves show a sharp crossing, allowing us to estimate the location of the critical point at $v_c = 0.0623(1)$ (the corresponding value of w_c is therefore $w_c = 0.1600(1)$). **(b)** $\Re(L) = \langle [\sum_{\vec{r}} \text{Re}(\psi^2(\vec{r}))]^2 \rangle / L^2$ scaled by $L^{2-\eta_2}$ as a function of v for different values of the system size L . The curves again cross at the value of v_c estimated above when η_2 is chosen as $\eta_2 = 0.70(5)$. (Inset) Scaling collapse of $\Re(L)/L^{2-\eta_2}$ using the value $\nu = 1.70$ for the correlation length exponent. Note that these estimates of η_2 and ν satisfy the Ashkin-Teller relation $\eta_2 = 1 - 1/(2\nu)$ within errors. **(c)** Scaling collapse with $\nu = 1.70(5)$ of Binder-ratio $\langle |\Psi_L|^4 \rangle / \langle |\Psi_L|^2 \rangle^2$ ($\Psi_L \equiv \sum_{\vec{r}} \psi(\vec{r})$) for various L .

of the critical point from the data displayed in the second figure. This gives us the estimate $v_c^* = 0.3180(3)$. This is fed back into our analysis of the data shown in the first figure, and used to collapse this data into a scaling collapse with ν as an adjustable parameter (displayed in Fig. 3 of main text). This yields the estimate $\nu^* = 0.92(3)$ quoted in the main text. The error-estimate is obtained by varying ν until the data collapse deteriorates appreciably. Finally, in the third figure, we show the L dependence of the alternate two-fold order parameter T defined in the main text for

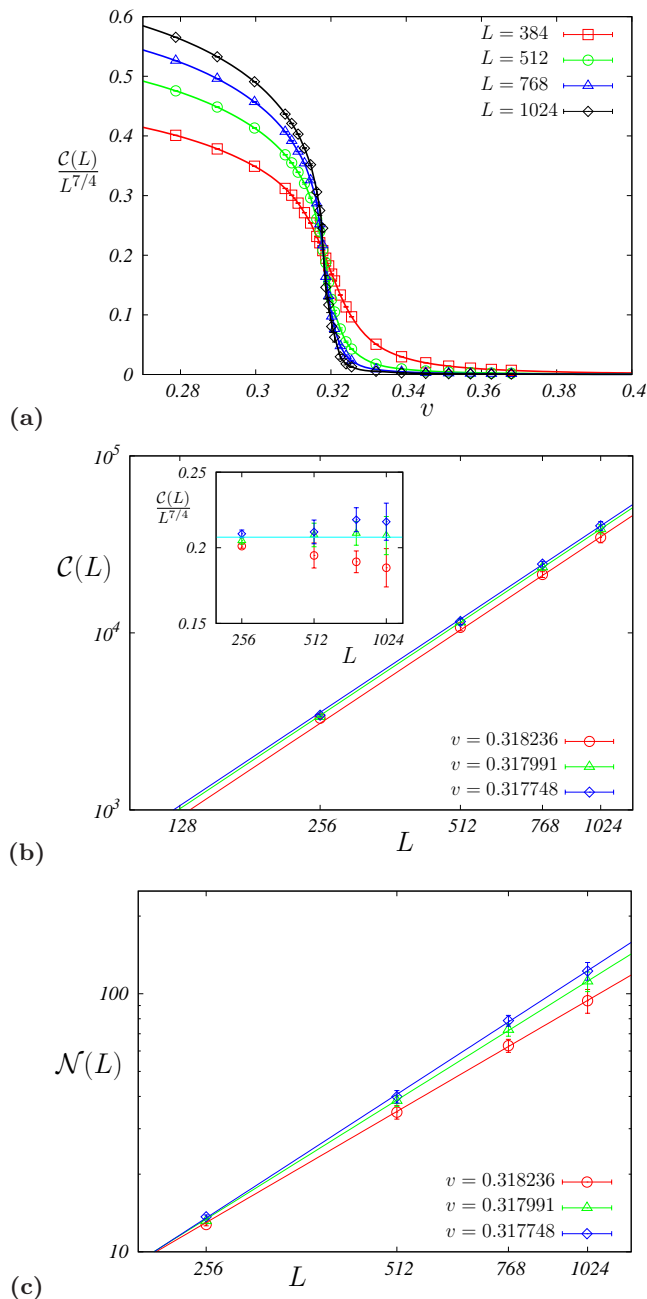


FIG. 8: Phase transition along *III* (the boundary *VS* with $w = 0$), corresponding to the hard-square lattice gas. **(a)** The figure shows the columnar order parameter $C(L) = \langle |\sum_{\vec{r}} \psi(\vec{r})|^2 \rangle / L^2$ scaled by $L^{7/4}$ plotted as a function of v for different values of the system size L . The sharp crossing seen is consistent with the fact that $\eta = \frac{1}{4}$ at this transition. Our estimate of the transition point is $v_c^* = 0.3180(3)$ (see data in next figure). **(b)** A precise estimate of the phase transition point v_c^* along *III* (the boundary *VS* with $w = 0$), is obtained by comparing the quality of power-law fits of $C(L)$ to the form $aL^{7/4}$ for various v in the critical region. The figure shows the data at three values of v along with the best power-law fit curves. The inset shows the L dependence of $\frac{C(L)}{L^{7/4}}$ at these three values. From this we see that the power-law fit to $aL^{7/4}$ works best at $v_c^* = 0.317991$ (this corresponds to $z_s = 97.8$, $z_v = 1$, $z_d = 0$ in the original parametrization of Z_{dsv}). The value quoted in the main text, *i.e.* $v_c^* = 0.3180(3)$, rounds off this value to four decimal places and includes an error estimate that corresponds to the spacing between the values of v at which we have measured this L dependence. **(c)** The figure shows the L dependence of $N(L) = \langle (\sum_{\vec{r}} T(\vec{r}))^2 \rangle / L^2$ (with $T(\vec{r})$ defined in main text) at three values of v in the critical region, along with the best-fit power-law curves $bL^{2-\eta_2}$ at these values of v . The best-fit values of the power-law exponent η_2 depends sensitively on the value of v in this critical region. We find that the postulated power-law fit works appreciably better at $v_c^* = 0.317991$ (identified in previous figure the power-law form $aL^{7/4}$) as compared to neighbouring values of v . The corresponding best-fit estimate of η_2 is $\eta_2^* = 0.46$.

the hard-square lattice gas. Fitting the L dependence of $\mathcal{N}(L) = \langle (\sum_{\vec{r}} T(\vec{r}))^2 \rangle / L^2$ to a power-law form $bL^{2-\eta_2^*}$ yields the estimate $\eta_2^* = 0.46(3)$ quoted in the main text. The error-bar on η_2^* is relatively large because of the sensitive dependence of the best-fit η_2 on the estimated value of v_c^* .

-
- [1] J. Kundu, R. Rajesh, D. Dhar, and J. Stilck, Solid State Phys. Proc. **57**, DAE Solid State Phys. Symposium 2011, AIP Conf. Proc. **1447**, 113 (2012).
 - [2] K. Ramola, TIFR thesis, unpublished (2012); available online at http://theory.tifr.res.in/Research/Thesis/Kabir-Ramola-PhD_Thesis.pdf
 - [3] J. Kundu, R. Rajesh, D. Dhar, and J. Stilck, Phys. Rev. E **87**, 032103 (2013).
 - [4] J. Kundu and R. Rajesh, Phys. Rev. E **89**, 052124 (2013).
 - [5] T. Nath and R. Rajesh, Phys. Rev. E **90**, 012120 (2014).
 - [6] X. Feng, H. W. J. Blote, and B. Nienhuis, Phys. Rev. E **83**, 061153 (2011).